Sensors and Actuators B 191 (2014) 806–812

Contents lists available at ScienceDirect

Sensors and Actuators B: Chemical

journal homepage: www.elsevier.com/locate/snb

Enhancement of NO_2 gas sensing response based on ordered mesoporous Fe-doped In_2O_3

Jing Zhao[a,b], Tianlin Yang[a], Yinping Liu[a], Zhenyu Wang[a], Xiaowei Li[a], Yanfeng Sun[a], Yu Du[c], Yuanchun Li[b], Geyu Lu[a,*]

[a] State Key Laboratory on Integrated Optoelectronics, College of Electronic Science and Engineering, Jilin University, 2699 Qianjin Street, Changchun 130012, China
[b] College of Electrical and Electronic Engineering, Changchun University of Technology, Changchun 130012, China
[c] Department of Applied Physics, Shenzhen University, Shenzhen 518060, China

ARTICLE INFO

Article history:
Received 15 April 2013
Received in revised form
27 September 2013
Accepted 30 September 2013
Available online 12 October 2013

Keywords:
Mesoporous
Indium oxide
Fe-doped
NO_2 sensor

ABSTRACT

Ordered mesoporous Fe-In_2O_3 has been synthesized via a nanocasting route using the three-dimensional (3D) cubic mesoporous KIT-6 silica as a hard template. Various techniques including X-ray diffraction (XRD), nitrogen adsorption–desorption and transmission electron microscopy (TEM) as well as X-ray photoelectron spectroscopy (XPS) were employed for the material characterization. All the results demonstrate that the obtained Fe-doped In_2O_3 displays the high surface area, ordered mesoporous structure and well crystallite. The NO_2 sensing properties of the sensors based on mesoporous pure In_2O_3 and Fe-doped In_2O_3 samples were detected by a static test system. The sensor utilizing mesoporous Fe-doped In_2O_3 exhibits much higher response to NO_2 gas compared to that using mesoporous pure In_2O_3 prepared by the same nanocasting technique. The excellent gas sensing property of mesoporous Fe-doped In_2O_3 is associated with its higher surface area and pore volume which induce highly effective surface interaction between the target gas molecules and the surface active sites. Moreover, the improved sensing behavior to NO_2 has been linked to the incorporation of iron species on the sensor, favoring the effective adsorption of NO_2 molecules on the surface. All the factors are obviously beneficial for enhancing the gas-sensing performance.

1. Introduction

NO_2, a typical pollution gas with pungent odor, generating from combustion chemical plants and automotive emissions, plays a major role in the formation of acid rain, photochemical smog and ground-level ozone, all of which are potentially harmful. The detection of nitrogen dioxide [1,2] becomes an exceedingly significant task for monitoring environmental pollution. Various types of techniques [3–7] have been developed to detect NO_2 gas, including semiconductor type, optical fiber, solid electrolyte gas sensor and laser-induced fluorescence instrument. Among them, gas sensors based on metal oxide semiconductor (MOS) [8–12] such as In_2O_3, Fe_2O_3, SnO_2, ZnO, and WO_3 are predominant gas detecting devices for domestic, laboratorial and commercial applications, owing to their miniaturization, easy fabrication, low cost, and good long-term stability. The mechanism [13,14] of semiconductor gas sensor is based on surface-chemical interaction between gas molecules and the sensor materials, thus, they are significantly influenced by the morphology and structure of sensing materials. However, the bulk materials or compact films with low specific surface areas limit the potential applications in gas sensing. Recently, significant research effort has been focused on improving the sensing performance of oxides semiconductor through manipulating their structure morphologies [15–18]. In particular, the ordered mesoporous metal oxides [19–23] synthesized through nanocasting strategy with hard templates have been established as a facile route to obtain gas sensing materials with optimized properties. Owing to their high specific surface area and ordered topological architecture, they can offer more active sites for oxygen adsorption and facilitate high accessibility for the gas molecules to the sensing materials.

Indium oxide, n-type semiconductor material with a wide band gap (E_g = 3.55–3.75 eV), plays an extraordinary role in a wide domain of useful applications, including gas sensor, catalyst, optoelectronic devices, as well as dye-sensitized solar cells. In_2O_3 as a promising candidate for gas sensor has been extensively applied in detecting NO_2 [24–27], O_3 [28], CH_4 [29], CO_2 [30] and C_2H_5OH [31]. In recent years, different synthesis routes have been developed to improve the sensing properties. Apart from increasing the specific surface area, the gas-sensing characteristics toward a particular

* Corresponding author. Tel.: +86 431 85167808; fax: +86 431 85167808.
E-mail address: Lugy@jlu.edu.cn (G. Lu).

0925-4005/$ – see front matter.
http://dx.doi.org/10.1016/j.snb.2013.09.118

target gas can also be further improved by surface modification [32–36], such as doping with Pd, Pt, Au, Cu, Fe or their oxides. The additives are chosen on the basis of their ability for enhancing the interaction between the target gas molecules and the sensing material.

Herein, we present an ordered mesoporous Fe-doped In_2O_3 prepared via the nanocasting route by using 3D cubic KIT-6 (space group Ia3d) mesoporous silica as a hard template, with indium and ferric nitrate salts as precursors. The morphological and structural properties of the material, as well as the chemical state of the additive are analyzed. The sensing properties of mesoporous pure In_2O_3 and Fe-doped In_2O_3 samples for NO_2 were measured. The introduction of metallic Fe is found to be effective to enhance the sensing characteristic of mesoporous In_2O_3 sensor toward NO_2, because the doping of iron species favors the effective adsorption of NO_2 on the sensor surface [37,38] and facilitates the reaction between oxygen species and NO_2 gas.

2. Experimental

2.1. Preparation of materials

The mesoporous KIT-6 silica with cubic Ia3d symmetry was prepared according to the previously report [39]. In a typical synthesis process, 6 g of Pluronic P123 ($EO_{20}PO_{70}EO_{20}$, MW = 5800, Sigma–Aldrich) was dissolved in 217 g of distilled water and 11.2 g of HCl (37%). Then, 6 g of butanol was added under stirring at 35 °C for 1 h. 12.9 g of TEOS was added into the above solution and subsequently the mixture was left under stirring for 24 h at 35 °C. The resulted gel was transferred into a closed Teflon-lined stainless steel autoclave and heated at 100 °C for another 24 h under a static condition. Finally, the solid product obtained after hydrothermal treatment was filtered off, washed with deionized water, dried at 100 °C and sintered at 550 °C for 6 h.

Mesoporous Fe-doped In_2O_3 was synthesized via nanocasting method. 1.72 g of $In(NO_3)_3{\cdot}4.5H_2O$ and 0.09 g $Fe(NO_3)_3{\cdot}9H_2O$ were dissolved in 10 ml of absolute ethanol. After stirring for 30 min, 0.5 g of KIT-6 was added to the above solution and stirring at 40 °C until all the solvent was evaporated, dried at 80 °C, and calcined at 300 °C for 3 h. To achieve higher loadings, the filling procedure was repeated following the same conditions but the amount of precursor was reduced by half. Sequentially, the resultant powder was calcined at 500 °C for 3 h. Finally, the silica template was removed using excess NaOH solution (2 M). The obtained slurry was centrifuged, copiously washed and dried. Mesoporous pure In_2O_3 was synthesized by a similar procedure.

2.2. Characterization

X-ray diffraction (XRD) patterns were recorded on a Rigaku D/MAX-2550 diffractometer using Cu-Kα radiation (λ = 0.15418 nm). Nitrogen adsorption-desorption isotherms were measured using a Micromeritics Gemini VII surface area and porosity system by high purity nitrogen as adsorbate at 77 K. The specific surface area was estimated by the five point Brunauer–Emmett–Teller (BET) method, and the pore size distribution was obtained by using the Barrett–Joyner–Halenda (BJH) analysis. Transmission electron microscopy (TEM) images were performed on a JEOL TEM-3010 instrument, operating at an acceleration voltage of 200 kV. Analysis of the X-ray photoelectron spectroscopy (XPS) was performed on Thermo ESCALAB 250 spectrometer.

2.3. Sensor fabrication and measurement

The as-synthesized samples were ground and mixed with deionized water in an agate mortar to form paste, and then the paste was coated onto an alumina tube on which a pair of Au electrodes was previously printed and Pt lead wires attaching to the Au electrodes were used for connecting with the measure instrument. Then, the devices were dried under IR radiation for 1 h, sintered at 500 °C for 2 h, and a Ni–Cr alloy coil was subsequently inserted into the alumina tube as a heater to keep the operating temperature. The sensing properties were carried out using a static test system, as diagrammed in Fig. 1, under laboratory conditions (40% ± 10% RH, 25 ± 1 c). The sensor was put into the test chamber, and a given amount of the target gas was injected into the test chamber for the measurement of the sensing performance. The electrical properties of the sensor were recorded by a digital multimeter (Fluke 8846A). The sensor response is defined as $S = R_a/R_g$ (reducing gas) and $S = R_g/R_a$ (oxidizing gas), where R_a is the resistance in air and R_g is the resistance in the target gas. The response and recovery time were defined as the time taken by the sensor to achieve 90% of the

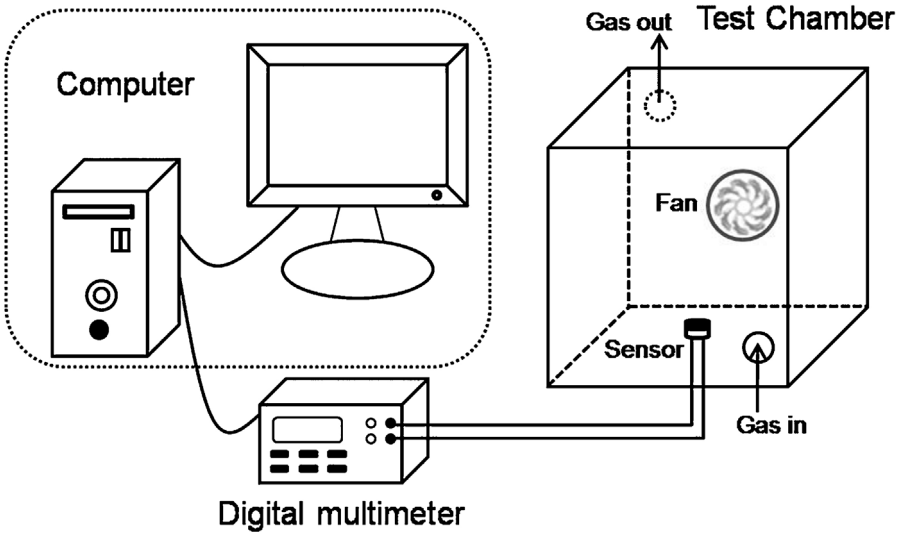

Fig. 1. Schematic illustration of sensor testing system.

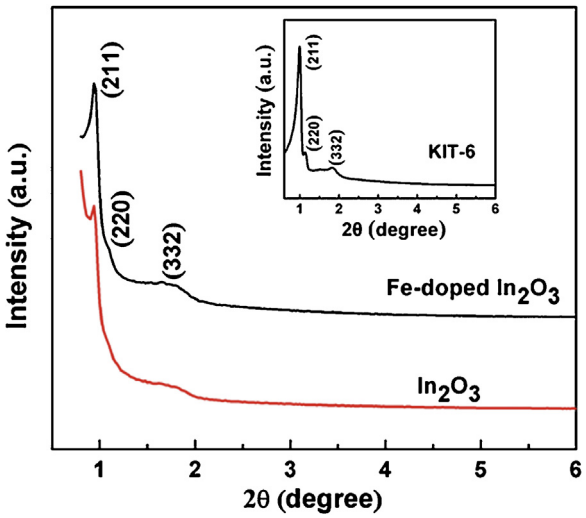

Fig. 2. Low-angle XRD patterns of mesoporous In_2O_3 and Fe-doped In_2O_3, as well as the hard template KIT-6 (inset).

total resistance change in the case of adsorption and desorption, respectively.

3. Results and discussion

3.1. Structure and morphology of as-prepared materials

Fig. 2 shows the low-angle X-ray diffraction (XRD) patterns of mesoporous In_2O_3 and Fe-doped In_2O_3 samples, as well as the hard template KIT-6 (inset). The patterns of In_2O_3 and Fe-doped In_2O_3 display the (2 1 1) (2 2 0) and (3 3 2) reflections, implying the samples are the negative replica of the KIT-6 silica matrix with periodically ordered cubic Ia3d symmetry mesostructure. In the case of KIT-6 matrix, the well-resolved diffraction is sharp, whereas the replicated In_2O_3 and Fe-doped In_2O_3 show somewhat broader and less well-resolved peaks, which indicate that the long-range order in the In_2O_3 and Fe-doped In_2O_3 samples are still rather low.

The wide-angle XRD patterns of mesoporous In_2O_3 and Fe-doped In_2O_3 samples are illustrated in Fig. 3(a). Both the diffraction patterns can be indexed to the body-centered cubic bixbyite-type crystalline phase In_2O_3 (JCPDS No. 06-0416), while no peaks were attributed to any iron or iron-based compounds in the patterns of the mesoporous Fe-In_2O_3 samples. The positions of the corresponding diffraction peaks from Fe-doped In_2O_3 sample are slightly shifted to higher angles compared to the pure In_2O_3 sample, especially for those corresponding to (2 2 2) plane, as shown in the enlarged partial view of the XRD patterns (Fig. 3(b)). The hardly discernable diffraction of Fe-related can be attributed to the Fe ions embedding into the In_2O_3 host structure. The lattice parameters of the mesoporous In_2O_3 and Fe-In_2O_3 were calculated to be 1.010 and 1.006 nm, respectively, which is consistent with the ionic radius of Fe^{3+} is smaller than that of In^{3+}. The crystallite size of samples can be calculated by the Scherrer equation [40],

$$D = \frac{0.9\lambda}{\beta \cos\theta} \quad (1)$$

where D is the crystallite size, λ is the wavelength of X-ray radiation, β is the full width at half-maximum intensity (fwhm in radians), θ is diffraction angle.

The average crystallite size of the mesoporous In_2O_3 and Fe-doped In_2O_3 are approximately 16.8 and 14.0 nm, respectively. All the well-resolved characteristic patterns indicate that well

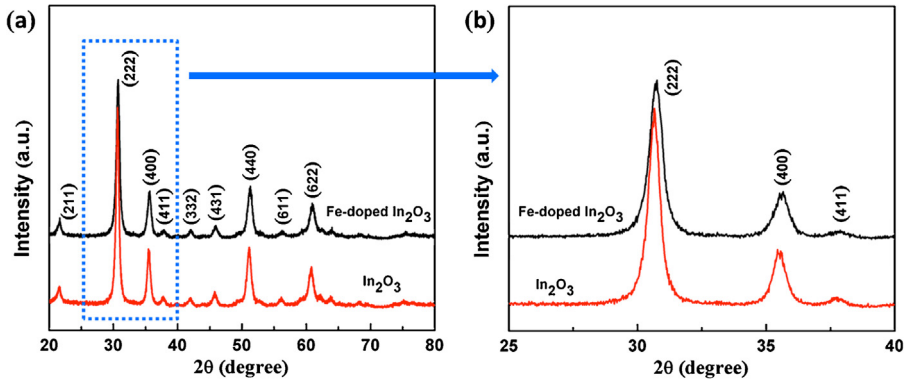

Fig. 3. (a) Wide-angle and (b) enlarged part XRD patterns of mesoporous In_2O_3 and Fe-doped In_2O_3.

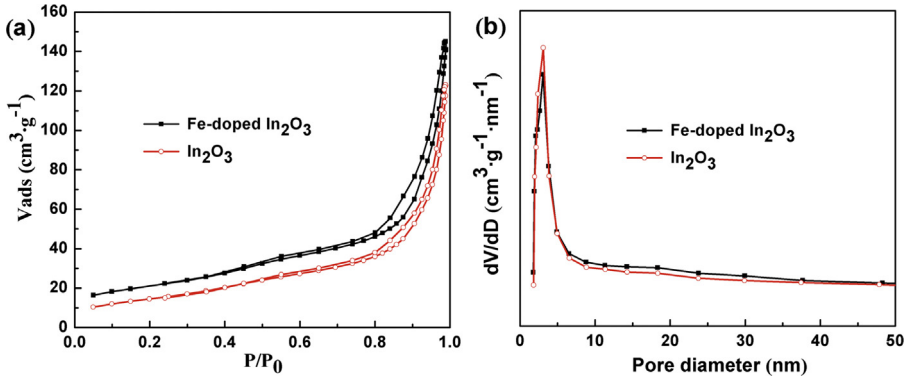

Fig. 4. (a) Nitrogen adsorption–desorption isotherms and (b) the corresponding pore size distribution of mesoporous In_2O_3 and Fe-doped In_2O_3.

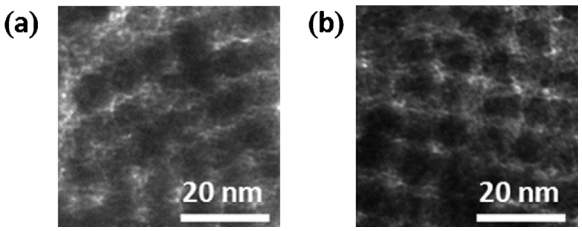

Fig. 5. TEM images of mesoporous (a) In_2O_3 and (b) Fe-doped In_2O_3.

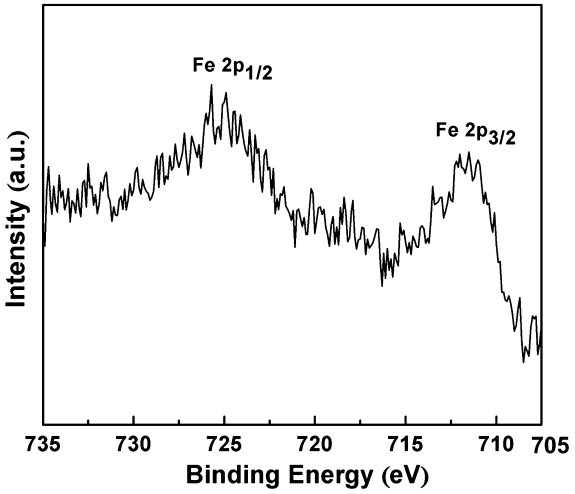

Fig. 6. XPS spectrum in the Fe 2p region of the mesoporous Fe-doped In_2O_3.

crystalline structure of the mesoporous In_2O_3 and Fe-doped In_2O_3 nanoparticles are obtained.

N_2 adsorption–desorption isotherms of mesoporous In_2O_3 and Fe-doped In_2O_3 samples are shown in Fig. 4(a). They all show typical type IV isotherms with hysteresis loops, which indicate that the obtained In_2O_3 and Fe-doped In_2O_3 samples exhibit the mesostructure. The corresponding pore size distribution of mesoporous In_2O_3 and Fe-doped In_2O_3 samples are displayed in Fig. 4(b). According to the BJH (Barrett–Joyner–Halenda) algorithm, the narrow pore size distribution of In_2O_3 and Fe-In_2O_3 calculated from the adsorption branch has a mean value approximately 3.0 nm and 3.2 nm. The BET surface area and the total pore volume of the mesoporous Fe-In_2O_3 are calculated to be 80.0 m^2/g and 0.24 cm^3/g, respectively, which are somewhat higher than that of pure mesoporous In_2O_3 (59.0 m^2/g and 0.22 cm^3/g).

The structures of mesoporous In_2O_3 and Fe-doped In_2O_3 were further characterized by TEM. In Fig. 5, the TEM images clearly show that all the samples exhibit distinguishable periodic ordering mesostructure and highly crystalline nanoparticles, indicating the successful replication from the silica templates. This feature suggests that these particles of samples regularly assemble together inside the pores of the hard template. All these characterization results confirm that ordered crystalline mesoporous In_2O_3 and Fe-doped In_2O_3 are obtained with a nanocasting route using KIT-6 silica as a hard template. In particular, the mesoporous In_2O_3 and Fe-doped In_2O_3 replica after heating at 500 °C for 3 h remains ordered mesostructure and high specific surface area, which suggests their good thermal stability.

The chemical state of the iron species has been investigated with X-ray photoelectron spectroscopy. As shown in Fig. 6, the binding energies of Fe $2p_{3/2}$ and Fe $2p_{1/2}$ are centered at 711.2 and 724.7 eV, respectively, indicating the existence of the Fe_2O_3 [41,42].

3.2. Sensing properties

The response of the sensors based on mesoporous In_2O_3 and Fe-doped In_2O_3 samples toward 1 ppm NO_2 were measured at various operating temperatures. As shown in Fig. 7(a), the maximum response of the sensor based on the mesoporous pure In_2O_3 is 27 at 100 °C and the response of mesoporous Fe-In_2O_3 sensor has reached to 116 at 100 °C. Obviously, the sensor based on mesoporous Fe-doped In_2O_3 exhibits much higher response than that of mesoporous pure In_2O_3 at each temperature. It is well known that the response time is also important parameter for evaluating the properties of gas sensor. The correlation between the response and response time of the mesoporous Fe-doped In_2O_3 sensor to 1 ppm NO_2 with the operating temperatures are shown in Fig. 7(b). The response time decreased dramatically, with the increasing of operating temperature. Such behavior indicates that fast response can be achieved by increasing the operating temperature. Therefore, balance of the higher response and faster response speed of the mesoporous Fe-doped In_2O_3 sensor, we have chosen 150 °C as the optimum operating temperature, which is applied in all the investigations hereafter. The transient response of the mesoporous Fe-doped In_2O_3 sensor to 1 ppm NO_2 was measured at 150 °C (Fig. 8), where the response is 71, as well as the response and recovery time is about 4.6 min and 2.5 min, respectively.

Fig. 9(a) shows the transient response of the mesoporous Fe-doped In_2O_3 sensor sequentially exposed to 0.04, 0.1, 0.2, 0.5, 1, 2, 5 and 10 ppm NO_2 at 150 °C. The response of the sensor increased with the increasing of the NO_2 concentration. It is worth noting that the sensor showed an obvious response to NO_2 concentration even as low as 40 ppb, and the response has reached to 6. Correspondingly, the response of mesoporous Fe-In_2O_3 sensor as a function of NO_2 concentration is displayed in Fig. 9(b). It increases rapidly with the increasing of gas concentration below 1 ppm. Though the

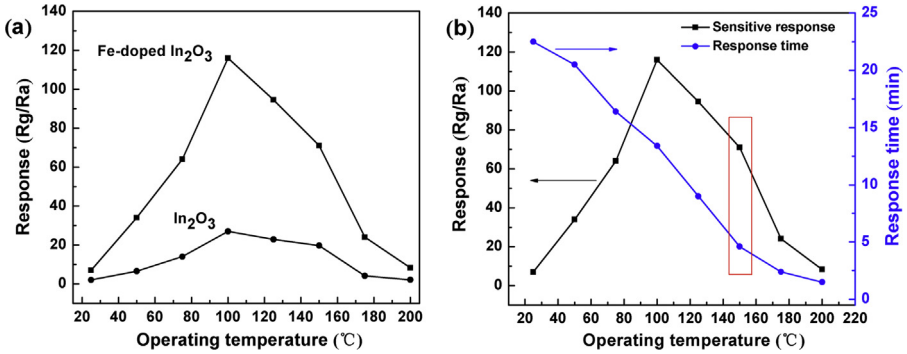

Fig. 7. (a) Response of the sensors based on mesoporous In_2O_3 and Fe-doped In_2O_3 samples toward 1 ppm NO_2 at various operating temperatures and (b) Correlation between the response and response time of the mesoporous Fe-doped In_2O_3 sensor to 1 ppm NO_2 with the operating temperatures.

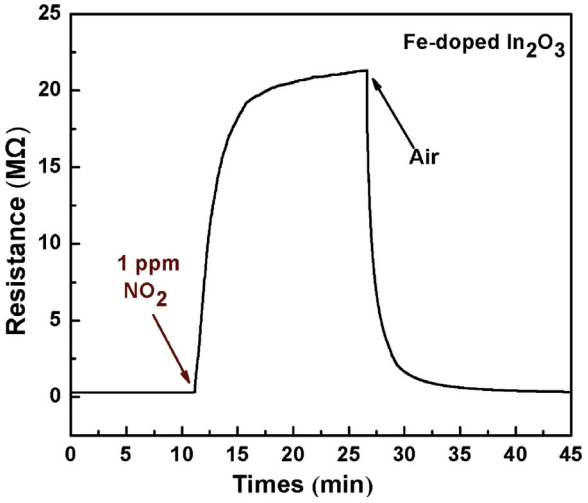

Fig. 8. Response and recovery of the mesoporous Fe-doped In_2O_3 sensor to 1 ppm NO_2 at 150 °C.

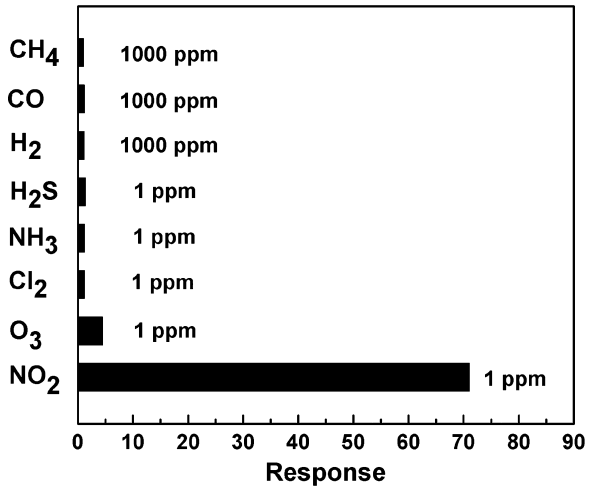

Fig. 10. Cross-sensitive response of the mesoporous Fe-doped In_2O_3 sensor to various gases.

response increases relatively slow when the NO_2 concentration is more than 1 ppm, it is not saturated until the concentration is up to 10 ppm, which indicates that the sensor is suitable for detection of NO_2 in a wide range. This unsaturation phenomenon to relatively high NO_2 concentration may be resulted from the high surface area and large pore volume of mesoporous Fe-doped In_2O_3 material, which provide abundant surface active sites and accommodate large number of target gas molecules.

The selectivity of the gas sensor is also important for practical application. Fig. 10 shows the cross-sensitive response of the mesoporous Fe-doped In_2O_3 sensor to various gases, including O_3, Cl_2, NH_3, H_2S, H_2, CO and CH_4. It is obvious that the mesoporous Fe-In_2O_3 sensor exhibits the largest response to NO_2 among the tested gases. Such result indicates that the sensor using the mesoporous Fe-In_2O_3 exhibits an excellent selectivity to NO_2 against the other tested gases.

The gas-sensing mechanism of n-type semiconductor sensor is mainly based on the electrical conductivity change originated from adsorption and desorption of gas molecules on the surface of sensing materials. When mesoporous Fe-In_2O_3 sensor is placed in air, the absorbed oxygen molecules will capture electrons from the sensor to generate chemical adsorption oxygen species (O_2^-, $O^-$and O^{2-}). The oxygen vacancies of the sensor as intrinsic electron donors provide electrons to the conduction band and extrinsic acceptors created by chemisorbed oxygen species result in the formation of a thick space-charge layer and depletion of free electrons in the near-surface region of each grain (depletion layer), lowering the overall electrical conductivity (increasing the resistance). When mesoporous Fe-doped In_2O_3 sensor is exposed to NO_2 gas, NO_2 can not only capture the electrons from the conduction band due to its higher electrophilic property but also react with the adsorbed oxygen species leading to the formation of adsorbed NO_2^- (ads). The mechanism can be explained by several chemical reactions which are shown below [2,43,44]:

$$NO_2(gas) + 2e^- \rightarrow NO^{2-}(ads) \quad (2)$$

$$NO_2(gas) + O_2^-(ads) + 2e^- \rightarrow NO_2^-(ads) + 2O^-(ads) \quad (3)$$

The above reactions decrease the carrier concentration and electron mobility on the sensor surface, which lead to the increase of depletion layer width and accompany with the increase of resistance.

The enhanced sensing properties of the mesoporous Fe-In_2O_3 sensor may be caused by higher surface area which can provide more active sites to react with the target gas, whereas an ordered mesoporous structure and high pore volume facilitates the adsorption and diffusion of NO_2 molecules. Moreover, incorporation of iron species on the sensor favors the effective adsorption of NO_2 on the surface. All the factors are obviously beneficial for the enhancement in gas-sensing properties, and thus the mesoporous Fe-doped In_2O_3 sensor exhibits a higher sensing response than that of mesoprous pure In_2O_3 sensor.

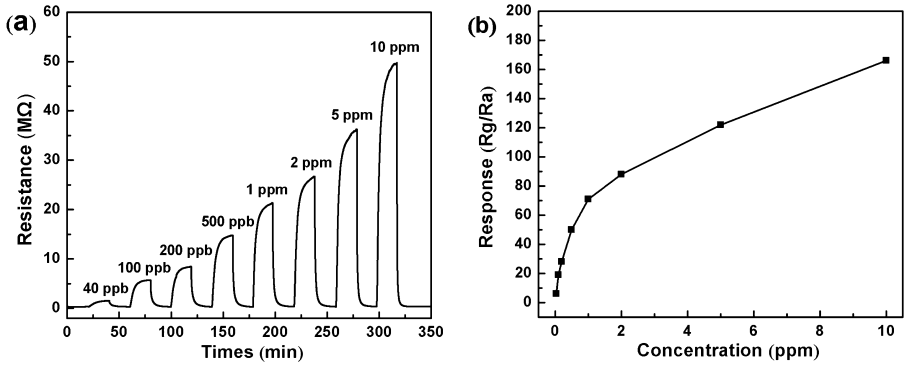

Fig. 9. (a) Transient response of the mesoporous Fe-doped In_2O_3 sensor to different NO_2 concentration at 150 °C and (b) Response of mesoporous Fe-In_2O_3 sensor as a function of NO_2 concentration.

4. Conclusions

In summary, the utilization of mesoporous KIT-6 silica as a hard template has turned out to be a versatile tool for the synthesis of mesoporous Fe-doped In_2O_3 in the nanocasting process. It exhibits high specific surface area, oredered periodically arranged mesoporous structure with well crystalline walls and high thermal stability. The product is a promising material for application as gas sensor, since its excellent physical and chemical properties. The gas sensing measurements reveal significantly increased sensitivity response to NO_2 gas in comparison with the mesoporous pure In_2O_3. It is supposed that the outstanding gas sensing properties of the mesoporous Fe-doped In_2O_3 sensor is attributed to higher specific surface area and the pore volume. Besides, Fe species loaded on the sensor is effective to adsorb NO_2 gas on the surface, which is also beneficial to the sensing performance of the sensor.

Acknowledgements

This work was supported by Natural Science Foundation of China (Nos. 61134010, 61074172, 21001051), Program for Changjiang Scholars and Innovative Research Team in University (No. IRT1017) and Jilin Province Science and Technology Development Plan Program (No. 20106002).

References

[1] Y. Shimizu, M. Egashira, Basic aspects and challenges of semiconductor gas sensors, MRS Bull. 24 (1999) 18–24.
[2] K. Wetchakun, T. Samerjai, N. Tamaekong, C. Liewhiran, C. Siriwong, V. Kruefu, A. Wisitsoraat, A. Tuantranont, S. Phanichphant, Semiconducting metal oxides as sensors for environmentally hazardous gases, Sens. Actuators B 160 (2011) 580–591.
[3] N.G. Cho, D.J. Yang, M.J. Jin, H.G. Kim, H.L. Tuller, I.D. Kim, Highly sensitive SnO_2 hollow nanofiber-based NO_2 gas sensors, Sens. Actuators B 160 (2011) 1468–1472.
[4] Ü. Kersen, Microstructural and surface characterization of solid state sensor based on $LaFeO_{3-\sigma}$ oxide for detection of NO_2, Analyst 126 (2001) 1377–1381.
[5] S. Ohira, P.K. Dasgupta, K.A. Schug, Fiber optic sensor for simultaneous determination of atmospheric nitrogen dioxide, ozone, and relative humidity, Anal. Chem. 81 (2009) 4183–4191.
[6] Q. Diao, C. Yin, Y. Liu, J. Li, X. Gong, X. Liang, S. Yang, H. Chen, G. Lu, Mixed-potential-type NO_2 sensor using stabilized zirconia and Cr_2O_3–WO_3 nanocomposites, Sens. Actuators B 180 (2013) 90–95.
[7] Y. Matsumi, S. Murakami, M. Kono, K. Takahashi, High-sensitivity instrument for measuring atmospheric NO_2, Anal. Chem. 73 (2001) 5485–5493.
[8] H. Jiang, J. Hu, F. Gu, W. Shao, C. Li, Hydrothermal synthesis of novel In_2O_3 microspheres for gas sensors, Chem. Commun. 24 (2009) 3618–3620.
[9] F. Rettig, R. Moos, α-Iron oxide: an intrinsically semiconducting oxide material for direct thermoelectric oxygen sensors, Sens. Actuators B 145 (2010) 685–690.
[10] F. Gyger, M. Hübner, C. Feldmann, N. Barsan, U. Weimar, Nanoscale SnO_2 hollow spheres and their application as a gas-sensing material, Chem. Mater. 22 (2010) 4821–4827.
[11] Z. Jing, J. Zhan, Fabrication and gas-sensing properties of porous ZnO nanoplates, Adv. Mater. 20 (2008) 4547–4551.
[12] N.V. Hieu, H.V. Vuong, N.V. Duy, N.D. Hoa, A morphological control of tungsten oxide nanowires by thermal evaporation method for sub-ppm NO_2 gas sensor application, Sens. Actuators B 171-172 (2012) 760–768.
[13] M. Epifani, J.D. Prades, E. Comini, E. Pellicer, M. Avella, P. Siciliano, G. Faglia, A. Cirera, R. Scotti, F. Morazzoni, J.R. Morante, The role of surface oxygen vacancies in the NO_2 sensing properties of SnO_2 nanocrystals, J. Phys. Chem. C 112 (2008) 19540–19546.
[14] J.T. McCue, J.Y. Ying, SnO_2-In_2O_3 nanocomposites as semiconductor gas sensors for CO and NO_x detection, Chem. Mater. 19 (2007) 1009–1015.
[15] S. Vallejos, T. Stoycheva, P. Umek, C. Navio, R. Snyders, C. Bittencourt, E. Llobet, C. Blackman, S. Moniz, X. Correig, Au nanoparticle-functionalised WO_3 nanoneedles and their application in high sensitivity gas sensor devices, Chem. Commun. 47 (2011) 565–567.
[16] X. Lai, J. Li, B.A. Korgel, Z. Dong, Z. Li, F. Su, J. Du, D. Wang, General synthesis and gas-sensing properties of multiple-shell metal oxide hollow microspheres, Angew. Chem. 123 (2011) 2790–2793.
[17] S. Deng, V. Tjoa, H.M. Fan, H.R. Tan, D.C. Sayle, M. Olivo, S. Mhaisalkar, J. Wei, C.H. Sow, Reduced graphene oxide conjugated Cu_2O nanowire mesocrystals for high-performance NO_2 gas sensor, J. Am. Chem. Soc. 134 (2012) 4905–4917.
[18] J.H. Lee, Gas sensors using hierarchical and hollow oxide nanostructures: overview, Sens. Actuators B 140 (2009) 319–336.
[19] J. Zhao, W. Wang, Y. Liu, J. Ma, X. Li, Y. Du, G. Lu, Ordered mesoporous Pd/SnO_2 synthesized by a nanocasting route for high hydrogen sensing performance, Sens. Actuators B 160 (2011) 604–608.
[20] T. Wagner, S. Haffer, C. Weinberger, D. Klaus, M. Tiemann, Mesoporous materials as gas sensors, Chem. Soc. Rev. 42 (9) (2013) 4036–4053.
[21] T. Wagner, C.D. Kohl, S. Morandi, C. Malagù, N. Donato, M. Latino, G. Neri, M. Tiemann, Photoreduction of mesoporous In_2O_3: mechanistic model and utility in gas sensing, Chem. Eur. J. 18 (2012) 8216–8223.
[22] E. Rossinyol, A. Prim, E. Pellicer, J. Arbiol, F. Hernández-Ramírez, F. Peiró, A. Cornet, J.R. Morante, L.A. Solovyov, B. Tian, T. Bo, D. Zhao, Synthesis and characterization of chromium-doped mesoporous tungsten oxide for gas-sensing applications, Adv. Funct. Mater. 17 (2007) 1801–1806.
[23] Y. Ren, Z. Ma, P.G. Bruce, Ordered mesoporous metal oxides: synthesis and applications, Chem. Soc. Rev. 41 (2012) 4909–4927.
[24] T. Hyodo, H. Inoue, H. Motomura, K. Matsuoa, T. Hashishin, J. Tamaki, Y. Shimizu, M. Egashir, NO_2 sensing properties of macroporous In_2O_3-based powders fabricated by utilizing ultrasonic spray pyrolysis employing polymethylmethacrylate microspheres as a template, Sens. Actuators B 151 (2010) 265–273.
[25] S. Kannana, H. Steinebachb, L. Rietha, F. Solzbachera, Selectivity, stability and repeatability of In_2O_3 thin films towards NO_x at high temperatures (≥500 °C), Sens. Actuators B: Chem. 148 (2010) 126–134.
[26] M.W.K. Nomani, D. Kersey, J. James, D. Diwan, T. Vogt, R.A. Webb, G. Koley, Highly sensitive and multidimensional detection of NO_2 using In_2O_3 thin films, Sens. Actuators B: Chem. 160 (2011) 251–259.
[27] P.S. Khiabani, E. Marzbanrad, C. Zamani, R. Riahifar, B. Raissi, Fabrication of In_2O_3 based NO_2 gas sensor through AC-electrophoretic deposition, Sens. Actuators B 166–167 (2012) 128–134.
[28] M. Epifani, E. Comini, J. Arbiol, E. Pellicer, P. Siciliano, G. Faglia, J.R. Morante, Nanocrystals as very active interfaces: ultrasensitive room-temperature ozone sensors with In_2O_3 nanocrystals prepared by a low-temperature sol–gel process in a coordinating environment, J. Phys. Chem. C 111 (2007) 13967–13971.
[29] T. Waitz, T. Wagner, T. Sauerwald, C.D. Kohl, M. Tiemann, Ordered mesoporous In_2O_3: synthesis by structure replication and application as a methane gas sensor, Adv. Funct. Mater. 19 (2009) 653–661.
[30] A. Prim, E. Pellicer, E. Rossinyol, F. Peiró, A. Cornet, J.R. Morante, A novel mesoporous CaO-loaded In_2O_3 material for CO_2 sensing, Adv. Funct. Mater. 17 (2007) 2957–2963.
[31] S.J. Kim, I.S. Hwang, J.K. Choi, Y.C. Kang, J.H. Lee, Enhanced C_2H_5OH sensing characteristics of nano-porous In_2O_3 hollow spheres prepared by sucrose-mediated hydrothermal reaction, Sens. Actuators B 155 (2011) 512–518.
[32] C. Liewhirana, N. Tamaekong, A. Wisitsoraat, A. Tuantranont, S. Phanichphant, Ultra-sensitive H_2 sensors based on flame-spray-made Pd-loaded SnO_2 sensing films, Sens. Actuators B 176 (2013) 893–905.
[33] B.J. Melde, B.J. Johnson, Mesoporous materials in sensing: morphology and functionality at the meso-interface, Anal. Bioanal. Chem. 398 (2010) 1565–1573.
[34] Y. Shimizu, E. Kanazawa, Y. Takao, M. Egashira, Modification of H_2-sensitive breakdown voltages of SnO_2 varistors with noble metals, Sens. Actuators B 52 (1998) 38–44.
[35] N. Yamazoe, G. Sakai, K. Shimanoe, Oxide semiconductor gas sensors, Catal. Surv. Asia 7 (2003) 63–75.
[36] T. Tesfamichael, A. Ponzoni, M. Ahsan, G. Faglia, Gas sensing characteristics of Fe-doped tungsten oxide thin films, Sens. Actuators B 168 (2012) 345–353.
[37] M. Ivanovskaya, D. Kotsikau, G. Faglia, P. Nellic, S. Irkaev, Gas-sensitive properties of thin film heterojunction structures based on Fe_2O_3–In_2O_3 nanocomposites, Sens. Actuators B 93 (2003) 422–430.
[38] A. Ueda, Y. Yamada, T. Kobayashi, Novel catalysts having NO_x-adsorption sites for the selective oxidation of ethane, Appl. Catal. A: Gen. 209 (2001) 391–399.
[39] F. Kleitz, S.H. Choi, R. Ryoo, Cubic Ia3d large mesoporous silica: synthesis and replication to platinum nanowires, carbon nanorods and carbon nanotubes, Chem. Commun. 213 (2003) 6–213, 7.
[40] S. Elouali, L.G. Bloor, R. Binions, I.P. Parkin, C.J. Carmalt, J.A. Darr, Gas sensing with nano-indium oxides (In_2O_3) prepared via continuous hydrothermal flow synthesis, Langmuir 28 (2012) 1879–1885.
[41] T. Yamashita, P. Hayes, Analysis of XPS spectra of Fe^{2+} and Fe^{3+} ions in oxide materials, Appl. Surf. Sci. 254 (2008) 2441–2449.
[42] X. Hu, J.C. Yu, J. Gong, Q. Li, G. Li, α-Fe_2O_3 nanorings prepared by a microwave-assisted hydrothermal process and their sensing properties, Adv. Mater. 19 (2007) 2324–2329.
[43] N.D. Hoa, N.V. Quy, D. Kim, Nanowire structured SnO_x–SWNT composites: high performance sensor for NO_x detection, Sens. Actuators B 142 (2009) 253–259.
[44] S. Bai, K. Zhang, R. Luo, D. Li, A. Chen, C.C. Liu, Low-temperature hydrothermal synthesis of WO_3 nanorods and their sensing properties for NO_2, J. Mater. Chem. 22 (2012) 12643–12650.

Biographies

Jing Zhao received her MS degree in physical chemistry in 2010 from Jilin University. She has been a PhD student at Jilin University since 2010, majored in microelectronics and solid state electronics. Her current research focuses on the synthesis and characterization of the functional materials and chemical sensors.

Tianlin Yang received her PhD from Electronics Science and Engineering Department, Jilin University, China in 2013. Presently, she is a lecturer of Changchun University of Technology, China. Her current research focuses on the nanoscience and chemical sensors.

Yinping Liu received her BS degree from the Electronics Information and Engineering Department, Jilin University, China in 2011. Presently, she is a graduate student, majored in integrated circuit Engineering.

Zhenyu Wang received his BS degree from the Electronics Science and Engineering Department, Jilin University, China in 2012. Presently, he entered the PhD course in 2012, majored in microelectronics and solid state electronics.

Xiaowei Li received his BS degree from the Electronics Information and Engineering Department, Jilin University, China in 2011. Presently, he is a graduate student, majored in integrated circuit Engineering.

Yan Feng Sun obtained his PhD from Jilin University of China in 2007. Presently, he is working as associate professor in Electronics Science and Engineering Department of Jilin University. His current research interests are nanoscience and gas sensors.

Yu Du received her PhD from chemistry of Jilin University, China in 2006. After that, she had been working as the Postdoctoral at NANYANG Technological University, Singapore for about two years. She is currently an Associate Professor at the Electronics Science and Engineering Department of Jilin University, China. Her current research interests are nanoscience and gas sensors.

Yuanchun Li received his Ph.D. at Harbin Institute of Technology, Harbin, P.R. China in 1990. Currently he is a full professor of Changchun University of Technology, Changchun, P.R. China. His main research interests include in dynamic modeling and control of complex systems, and robotic control.

Geyu Lu received his BS and MS degree in electronic sciences from Jilin University, China in 1985 and 1988, respectively, and PhD degree in 1998 from Kyushu University in Japan. Now he is a professor of Jilin University, China. Presently, he is interested in the development of functional materials and chemical sensors.